JGR Space Physics

METHOD
10.1029/2022JA031050

Key Points:

- Using new data from ICEBEAR 3D, we find that ionospheric turbulence overlap with meteor trail echoes between 90 and 110 km altitude
- The starkly different patterns of clustering in time and space of high latitude ionospheric turbulence and meteoric echoes are used to distinguish the echo types
- The spatial and temporal separation between observed meteor trail echoes is normally several orders of magnitude above that of ionospheric turbulence echoes at high latitudes

Correspondence to:
M. F. Ivarsen,
m.f.ivarsen@fys.uio.no

Citation:
Ivarsen, M. F., St-Maurice, J.-P., Hussey, G. C., Galeschuk, D., Lozinsky, A., Pitzel, B., & McWilliams, K. A. (2023). An algorithm to separate ionospheric turbulence radar echoes from those of meteor trails in large data sets. *Journal of Geophysical Research: Space Physics*, *128*, e2022JA031050. https://doi.org/10.1029/2022JA031050

Received 26 SEP 2022
Accepted 16 DEC 2022

An Algorithm to Separate Ionospheric Turbulence Radar Echoes From Those of Meteor Trails in Large Data Sets

Magnus F. Ivarsen[1,2], Jean-Pierre St-Maurice[1,3], Glenn C. Hussey[1], Draven Galeschuk[1], Adam Lozinsky[1], Brian Pitzel[1], and Kathryn A. McWilliams[1]

[1]Department of Physics and Engineering Physics, University of Saskatchewan, Saskatoon, SK, Canada, [2]Department of Physics, University of Oslo, Oslo, Norway, [3]Department of Physics and Astronomy, University of Western Ontario, London, ON, Canada

Abstract Coherent scatter echoes from disintegrating meteors and from the unstable ionospheric E-region can overlap considerably between 90 and 110 km altitudes. As the physical origin of plasma irregularities produced by meteor trails differs starkly from that of E-region auroral irregularities, this has consequences for winds as well as electrodynamic studies, thereby introducing a need to distinguish between the two types of echoes. To that goal, we have developed a novel separation algorithm to automatically sort through arbitrarily large data sets in the region of overlap. This proves very useful when the 3D location of echoes is available. The algorithm uses a definition of crowding, or clustering, in both time and space and has been developed and tested with a comprehensive data set obtained from the recently built Canadian ICEBEAR 3D radar. We discuss the characteristics belonging to the two classes of echoes, and present statistical results about the location of each type of echo as a function of conditions. Our proposed algorithm can be applied to any coherent scatter echo data with high resolution 3D location information.

Plain Language Summary Radars measure turbulence in space plasma by bouncing a signal off of sharp plasma density gradients in the ionosphere. For decades, such coherent radars have been useful tools to investigate the ionosphere. However, when probing E-region plasma, a coherent radar will pick up plasma produced by meteors as they enter Earth's atmosphere. We have developed an automatic algorithm to separate meteor trail echoes, as they are called, from space plasma measurements. We demonstrate the efficiency of this algorithm on the ICEBEAR 3D data set, which has an unprecedented resolution, and offers accurate 3D location data for space plasma turbulence.

1. Introduction

Radio-waves are used routinely to probe the upper atmosphere and ionosphere. With ground based transmitters, ionosondes study the altitude at which the transmitted frequency matches the ionospheric plasma frequency at which point they are reflected back, thereby providing very useful information about ionization profiles (Hargreaves & Hunsucker, 2002). Radars are also used to study structures with scale lengths of the order of the radar wavelength. So-called incoherent scatter radars are so powerful that they can sample small amplitude structures associated with the plasma when it is in thermal equilibrium. On the other hand, coherent radars require much less transmit power as they use radio waves scattered by much larger amplitude structures than when the plasma is in thermal equilibrium. Of interest to the present work are large amplitude structures generated by meteor trails (McKinley, 1961) and by ionospheric turbulence generated by plasma instabilities. The latter class can be particularly strong in the auroral region at times (Chau & St.-Maurice, 2016; Hysell, 2015; Larsen et al., 2007).

In the auroral E-region, at least at times, several plasma instability processes cause large amplitude irregularities all the way to wavelengths less than 1 m in size (Abel & Newell, 1969; St. Maurice et al., 1989). Above 20 MHz and with electric fields in excess of 20 mV/m the Farley-Buneman instability (Buneman, 1963; Farley, 1963) is the main source of irregularities behind coherent scatter observations (Hysell, 2015). Other instabilities are also possible (e.g., the gradient-drift instability), but unless there are large current densities along the geomagnetic field, which seems relatively rare, the resulting irregularities are all strongly aligned with the geomagnetic field (St-Maurice & Hamza, 2009). The instabilities are also facilitated by Hall currents, which also means that the altitudes will typically be between 100 and 120 km. With the Earth's magnetic field being nearly vertical at

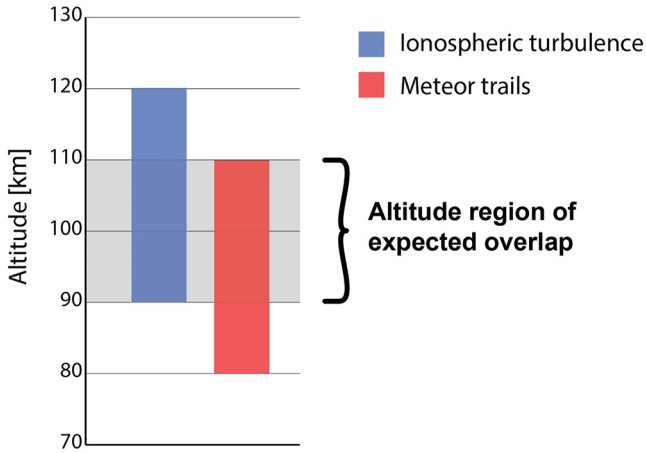

Figure 1. Schematic diagram showing the expected altitudes for ionospheric turbulence radar echoes and for those of meteor trails, highlighting the altitude region of expected overlap between the two.

auroral latitudes, this means that E-region irregularities associated with Hall currents will be detected at low-elevation angles at high-latitudes (Chau & St.-Maurice, 2016; Haldoupis, 1989).

A separate source of coherent radar echoes is meteors. As they enter Earth's dense atmosphere and burn up, new plasma is created along the meteor path. In the simplest instance, the newly created plasma diffuses away from the center of that path, producing long cylinders of plasma with a radius that keeps expanding according to diffusion (Kero et al., 2019; McKinley, 1961). There are many complications beyond this simple description in which case the echoes are called "non-specular." For instance the trail may develop kinks so that interference between trail elements will occur, leading to fading events. Sometimes, the meteors produce so-called overdense echoes which are long lived because the newly created plasma is denser than usual. In that case reflection of plasma waves is seen in lieu of Bragg scattering. On top of all this, if very high resolution measurements are made, head-on echoes maybe observed, not to mention short lived but intense plasma instabilities (Oppenheim, Dyrud, & Ray, 2003). For the most part, however, a coherent radar normally does not have the time resolution or sensitivity to observe such transients, while fading or interference between broken pieces of meteor trails seems to be far from being as frequent as the specular echoes obtained from expanding cylindrical plasmas.

Most echoes from meteors in ordinary coherent radar systems are assumed to simply decay according to diffusion in long cylinders. Fourier analysis of the diffusion equation predicts that the density at a given wavenumber k obtained from Bragg scattering decays according to the diffusion equation (e.g., Moisan & Pelletier, 2012)

$$n = n_0 \exp\left(-k^2 D\right) = n_0 \exp\left(\frac{-k^2 K_b T}{m\nu}\right) \quad (1)$$

where D is the diffusion coefficient and often assumed to be given by $K_b T/(m\nu)$ where K_b is the Boltzman constant, T is the temperature, m the ion mass for the plasma created by the crashing meteor (normally NO^+ or O_2^+) and ν is the collision frequency with neutrals. If the decay rate is too fast (small collision frequency), scattering by meteor trails is short lived or too weak to register. This introduces an upper altitude in the recording of meteor echoes that goes down as the radar frequency increases.

Needless to say, meteor echoes are therefore not really associated with ionospheric turbulence after an initial fast transient. For the most part the trails are pushed by the neutral winds, meaning that meteor trails are used a lot to monitor mesospheric winds (e.g., Hall et al., 1997; Hussey et al., 2000; Jenkins et al., 1998; Kumar, 2007; Yukimatu & Tsutsumi, 2002). They are also used to monitor the neutral density through the diffusion time constant (Stober et al., 2012, 2014).

Given the constraints imposed by the burnout altitude and diffusion, *most* meteor trail echoes are observed at altitudes ranging between 80 and 110 km (Barnes, 1973; Bourdillon et al., 2005; Sugar et al., 2010), though meteor trails have been observed at altitudes up to 170 km (Li et al., 2014). This means that there is a considerable overlap between meteor trail echoes and the E-region ionosphere, as E-region plasma instabilities triggered by currents in combination with density gradients can exist at altitudes as low as 90 km and as high as 120 km (St.-Maurice & Chau, 2016). The expected region of overlap is schematically shown in Figure 1. As the physical origins and resulting information retrieved from radar echoes produced by meteor trails on the one hand and E-region auroral irregularities on the other differ starkly, there is therefore a need to distinguish between the two types of echoes.

One approach used to distinguish meteor echoes from plasma turbulence is based on exploiting the differences in Doppler spectral properties between the two types. This was done, for example, with the SuperDARN HF radar network (e.g., Jenkins et al., 1998; Li et al., 2021). This being stated, recall that less frequent non-specular echoes which might be associated with fading or temporary turbulence will produce spectra not easily distinguishable from those of E-region irregularities generated by the turbulence from Hall currents (Oppenheim, Dyrud, & vom Endt, 2003). Another approach has been used with SuperDARN to distinguish meteor trail echoes through a

modification of the software used to analyze incoming data, focusing on quick timescales during which meteor trails decay (Yukimatu & Tsutsumi, 2002).

With the advent of increasingly versatile coherent radars capable of fine 3D echo localization, the need for a method to detect the physical origin of radar echoes around 100 km altitude is becoming more pressing. Here we elaborate on a method based on the clustering of echoes in time and space, which eliminates the difficulties associated with the fact that meteor trail and ionospheric turbulence echoes can have similar Doppler shifts, in addition to similar Doppler spectral widths. In one of the first studies to distinguish between meteor trail echoes and ionospheric turbulence echoes with this approach, Hall et al. (1997) used SuperDARN range-time-intensity plots to point out that meteor were introducing "grainy near-range echoes" in contrast to ionospheric turbulence. The graininess was only seen at short range, that is, at altitudes less than 120 km, which matched expectations for meteor echoes. It furthermore indicated that meteor echoes appear isolated both in space and time. Using novel plasma irregularity backscatter observations from the ICEBEAR 3D data set, we are now in a position to build upon this expectation, based on each incoming echo's spatial position as a function of time.

Our tool for the present study will be the Ionospheric Continuous-wave E region Bistatic Experimental Auroral Radar, or ICEBEAR, which is a coherent scatter radar operating in Saskatchewan, Canada, at a frequency of 49.5 MHz (Huyghebaert et al., 2019). The receiver and transmitter locations are separated by ∼240 km, allowing for the continuous wave operation mode. During Summer 2019, ICEBEAR was reconfigured to produce the ICEBEAR 3D data set. The reconfiguration entailed improvements in the software processing of the ICEBEAR echoes, and a physical reconfiguration of the antenna positions (Galeschuk, 2021; Lozinsky et al., 2022). As a result, ICEBEAR 3D now offers unprecedented resolution in altitude and azimuthal angle, along with a particularly wide field of view.

In what follows, we present our new technique for the classification of backscatter echoes based on their physical origin. Our algorithm can automatically classify millions of echoes based solely on their tendency to *cluster* in time and space. The algorithm is simple, yet powerful, and we demonstrate its capability under various conditions. While exceptions to this method show up, the rules for very large data sets are clearly illuminated by the proposed algorithm. We trained the algorithm on the ICEBEAR 3D data set. We then produced a quick survey from a statistical analysis of radar echoes below 130 km altitude, after they had been separated into their meteor echoes and plasma turbulence echo components.

2. Methodology

2.1. ICEBEAR 3D Data Set

The database used in the present study is the Level 2 ICEBEAR 3D data product, which consists of timeseries of echo locations (latitude, longitude, altitude), along with echo Doppler shift and signal-to-noise ratio (SNR).

Before using the data for the purpose at hands, some artifacts first had to be cleared. Both as a first introduction to the ICEBEAR 3D database, and as an explanation for the initial data sanitation procedure that was needed, we present in Figure 2 a view of 162 million echoes recorded during 2020, 2021, binned by azimuth and elevation angles. These are all the echo positions generated by the original algorithm described in Lozinsky et al. (2022), and contour lines of constant altitude indicate at which altitude the algorithm determines the echoes to be coming from. In panel (a), we immediately observe that, for the most part, echoes cluster in three distinct low-elevation beams. These are a result of the various null regions in the receiver-transmitter antenna patterns, and due to the 3λ (wavelength) spacing of the two transmitter antennas. We dub these three regions the west, center and east beams.

In between the three main beam regions the generally weak power echoes that were identified turned out to exhibit Doppler shifts that were completely different from the rest, indicating analysis problems in the null regions, due to a complete lack of transmitted power in those regions. In addition the data indicated that there were three altitude echo regions centered 100, 200, and 400 km altitudes, shown by the echo density occurring near the relevant black contour lines tracing constant echo altitude. These much less frequent recordings were also aligned with the beam pattern. The altitude regions above 150 km could well be spurious (looking like echoes of echoes) and once again seem to be an artifact of the analysis technique. We simply removed these higher altitude regions from the data set, given that the research for the radar at hand was strongly focusing on E region echoes from below 120 km altitude, be they from turbulence associated with Hall currents, or of meteoritic origin. We have

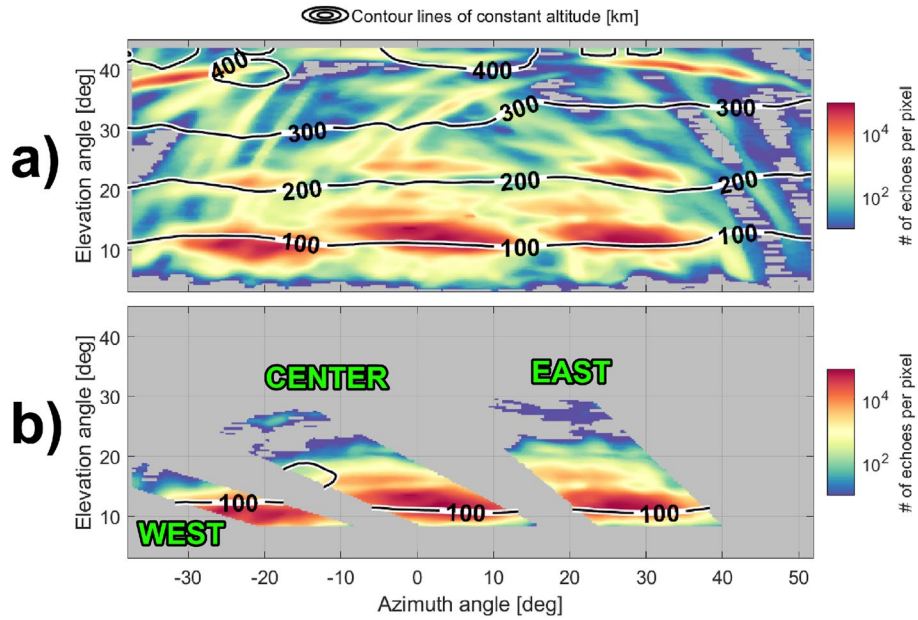

Figure 2. ICEBEAR 3D echo number density binned by azimuth angle (*x*-axis) and elevation angle (*y*-axis), shown with a logarithmic color scale. Contour lines of constant altitude are indicated by solid black lines. Panel (a) shows all echoes recorded during 2020, 2021, while panel (b) shows the three-beam configuration with an altitude cut-off implemented. Black contour lines are traced for the altitudes of 100, 200, 300, and 400 km (panel a) and 100 km (panel b).

therefore removed all echoes from 150 km altitude and above, thereby allowing for possible needed adjustments up to 150 km in case of potentially unknown details in the beam pattern (more on this and how to deal with those echoes is described in a follow-up paper).

Below the three beams, there is also a low-density area of very low-altitude (less than 70 km) echoes. These were also excluded from the database, given that we would expect that the vast majority of meteoroids to already have disintegrated by then (Barnes, 1973; Bourdillon et al., 2005; Sugar et al., 2010). In the end, therefore, we excluded from the database all echoes from below 70 km and above 150 km altitudes and all echoes originating from the null regions *between* the three beams, where echo altitudes, Doppler shifts and SNR tend to be spurious and anomalous. The result of this purge is shown in Figure 2b, where we label each beam with green lettering.

The data sanitation procedure led to a reduction in the size of the original level 2 data set to 131 million echoes, compared to the original 163 million or roughly a 20% reduction. As can be seen from the 100 km-altitude contour line in Figure 2b, we still see somewhat lower altitudes from the west beam compared to the other two beam, which appears to be related to an anomaly in the antenna beam pattern. We therefore considered the three beams separately in our classification algorithm. In the next subsection we describe the proposed algorithm for the classification of ICEBEAR 3D echoes according to their physical origin.

2.2. The Echo Classification Algorithm

Figure 3a presents a 14-hr sample of ICEBEAR 3D data for which the radar recorded 286,000 echoes on 19 February 2021. The location of median Doppler shift data inside small data bins is plotted in geomagnetic coordinates, with magnetic latitude (MLAT) along the *y*-axis and magnetic longitude along the *x*-axis, using the altitude-adjusted corrected geomagnetic coordinates system (Baker & Wing, 1989). The median echo Doppler shift in each MLON-MLAT bin is plotted with an appropriate color scale, with red-shifted echoes receding from the observer. For the 14-hr interval in question, there are two distinct Doppler shift populations with a slow more dispersed population of echoes at MLATs lower than ~65°, predominantly on eastern MLONs. The faster Doppler shift population occupies higher MLATs in the west and center beams. A small population of the faster echoes has Doppler shift magnitudes in the vicinity of 500 m/s.

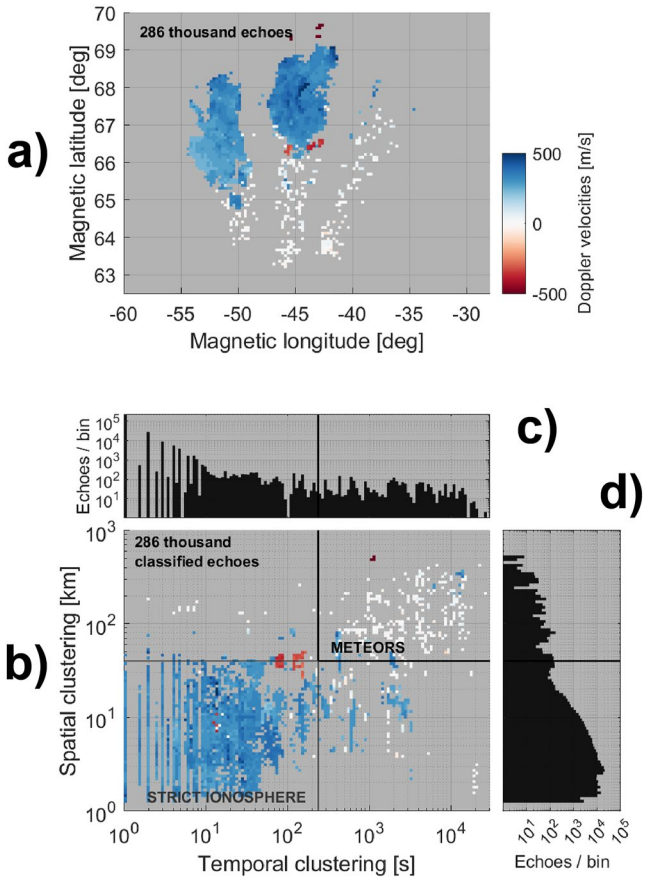

Figure 3. Data from ICEBEAR 3D echoes that were recorded during 14 hr of operation on 19 February 2021 between 16 and 6hr magnetic local time while passing through midnight. A total of 286,000 echoes were recorded for the event. Panel (a) median Doppler shift values as a function of binned echo locations in geomagnetic space, with magnetic longitude along the *x*-axis and magnetic latitude along the *y*-axis. The color scale for the median Doppler shift is also shown. Panel (b) Doppler shift as a function the space and temporal clustering scales. Panel (c) temporal clustering distribution integrated over all spatial cluster scales. Panel (d) spatial clustering distribution integrated over all temporal cluster scales. Black solid lines in panels (b) (c), and (d) indicate the threshold values distinguishing between the "strict ionosphere" and "meteor trail" echo classifications. The regions were identified using echoes from all three beams.

Meteor trails should rarely have Doppler shifts in excess of 90 m/s if coming from the dominant population of specular echoes, and even the non-specular kind could be similarly slow (McKinley, 1961). The reason is that the trails that produce specular echoes are carried by the neutral atmospheric winds, which below 110 km are for the very most part less than 100 m/s in magnitude even at high latitude (Larsen, 2002). By contrast, ionospheric irregularities produced by the Farley-Buneman instability should exhibit Doppler shifts that reach up to the ion-acoustic speed which should be 400 m/s or greater depending on altitude and electric field strength (St.-Maurice & Chau, 2016). We therefore expect that the faster echoes (blue dots) in Figure 3a should be associated with the Hall-current driven Farley-Buneman instability while the slower echoes (white dots) could be either from meteors or mode-coupling induced secondary waves associated with Farley-Buneman turbulence (St-Maurice & Hamza, 2009). A "graininess" algorithm of the type initially formulated by Hall et al. (1997) should therefore be able, if successful, to clearly identify the faster echoes as being from ionospheric turbulence and to identify a good portion of the slow Doppler shifts as coming from meteor trails.

Inspired by the granularity concept, we have developed a simple algorithm to automatically classify echoes of the type seen by ICEBEAR 3D. We started by defining spatial clustering as the median distance between each echo and its 512 nearest neighbors in space, calculated in a 4-hr window, using intra-echo distances projected on a spherical shell around the Earth at 105 km altitude. Similarly, we define temporal clustering as the median *temporal* distance between each echo and its 512 nearest neighboring echoes in time. In both these definitions, no binning is performed, and each echo is considered in relation to its neighbors in time and space, and this process is greatly facilitated by the rather accurate 3D positioning of each echo. Based on the clustering calculations, Figure 3b shows the Doppler shift and actual arrangement of all the echoes from panel (a), this time binned by temporal (*x*-axis) and spatial (*y*-axis) clustering, in a log-log representation. The overall echo distributions in temporal and spatial clustering are also shown in panels (c) and (d) respectively. We observe that in panel (b), the distributions of the Doppler shifts are quite separate, with the top right corner detached from the rest: this latter population is associated with the "grainy meteor trail echoes." It reflects that meteor trails clearly have a larger separation between them in time and space by contrast with irregularities produced by Hall currents, which are excited basically uniformly over a wide region of space and time, thereby implying a much tighter cluster than meteor trail echoes. This notion was of course verified during days for which there were meteor echoes and no auroral radar echoes in the field-of-view and vice versa, when there were only few meteor echoes and very strong auroral echoes.

The last point has taken us to formulate a criterion to distinguish between the two classes of echoes: if the distribution of echoes in the clustering plane (Figure 3b) is clearly separable into two diagonally distinct distributions, we define the echoes belonging to the bottom left as ionospheric turbulence, and the top right as meteor trail echoes. For some events, however, there might either be little to no ionospheric turbulence or, on the contrary, too few meteor echoes. In those cases, there might be no clearly separable distribution. However, through the testing of numerous large data sets we have been able to establish the threshold values to be 200 s for the temporal clustering, and 40 km for the spatial clustering. Of course, exceptions have to be acknowledged, though they won't matter for statistical studies. These exceptions would be if the Hall currents are too small or only marginally large enough to excite Farley-Buneman types of instabilities, or if, by contrast, there was a very intense meteor shower with much tighter clustering than the norm. Such events when identified should be treated separately from the rest.

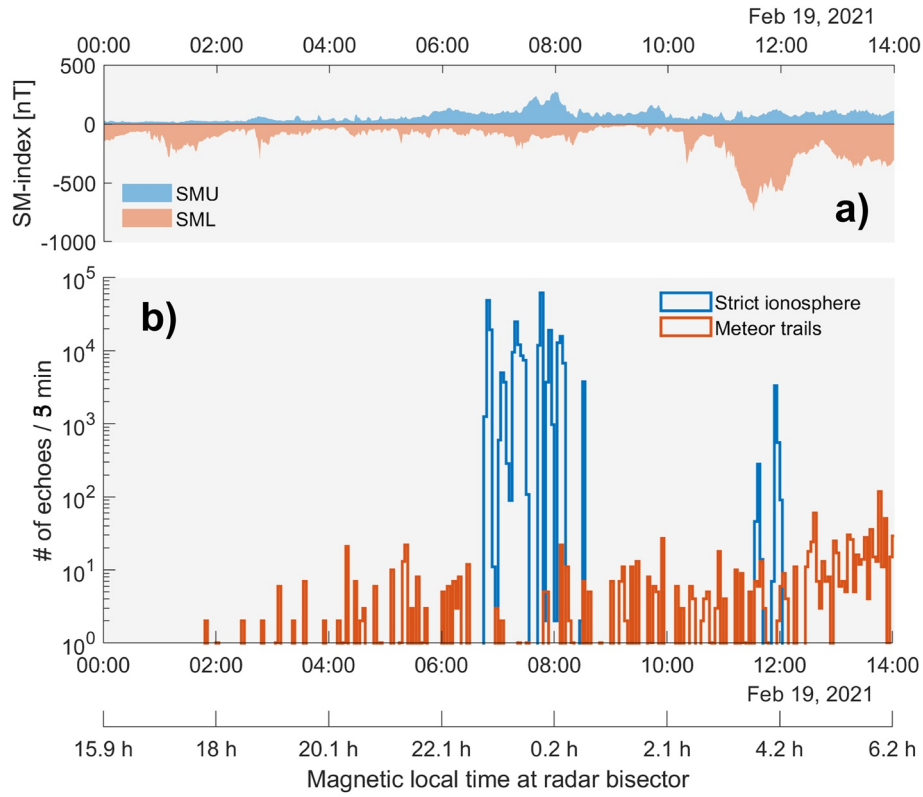

Figure 4. Panel (a): The upper (shows the upper, blue) and lower (shows the lower, orange) envelope of a magnetic disturbance index, the SM-index, for 19 February 2021. Panel (b): Rate of incoming echoes for all 14 hr of ICEBEAR operation on 19 February 2021, measured by number of echoes per 5 min. Strict ionospheric echoes are shown in blue while meteor trail echoes are shown in orange.

Three natural classes of echoes emerge from Figure 3b: the class of echoes that are highly clustered in space and time can be designated as "strict ionosphere." Second, echoes that are clustered in either space or time (but not both) are designated as being "unclassified echoes." Finally, the class of echoes that do not cluster tightly either in time or space (top right in Figure 3b) are designated as meteor trail echoes. Lastly, since their Doppler shifts are too large to normally be from neutral winds deemed meteor trail echoes that are faster than 90 m/s in Doppler shift magnitude are also classified as "unclassified echoes." These might be from anomalies in the neutral winds or come from a non-specular subpopulation. Also, there could occasionally be short spiky electric field events that would introduce larger temporal clustering, perhaps near the boundary of an ionospheric echo region. Finally, we note that the time-separation between an echo and its 512 nearest neighbor could be zero if neighboring echoes are triggered at the same time within the temporal resolution of the instrument; for this reason, in Figure 3b, we assign a lowest median separation of 1 s to fit in the log-log representation of the figure, which is coincidentally also the ICEBEAR 3D temporal resolution.

Going back to Figure 3, we see that the vast majority of echoes fall in the "strict ionosphere" class for the sample day that was chosen, although a small proportion of echoes are classified either as meteor trail echoes or as unclassified echoes. The unclassified echoes can conceivably be both meteoric and ionospheric in origin. While meteor trails that move with the neutral wind will not exhibit fast Doppler shifts, there are exceptions for meteors that break into several objects, producing non-specular echoes. Such non-specular echoes will exhibit unusual Doppler shifts owing to fading from self-clutter (Oppenheim, Dyrud, & vom Endt, 2003). Some of the unclassified echoes might come from episodes that are more crowded in time and space, as the meteor trails in question might be longer lived, being associated with larger objects to start with. The algorithm then errs on the side of caution; fast (>90 m/s) echoes in the meteor trail class are "unclassified" echoes. When dealing with large statistical studies of the E-region ionosphere we adopted the safest approach, namely, only kept echoes that fell

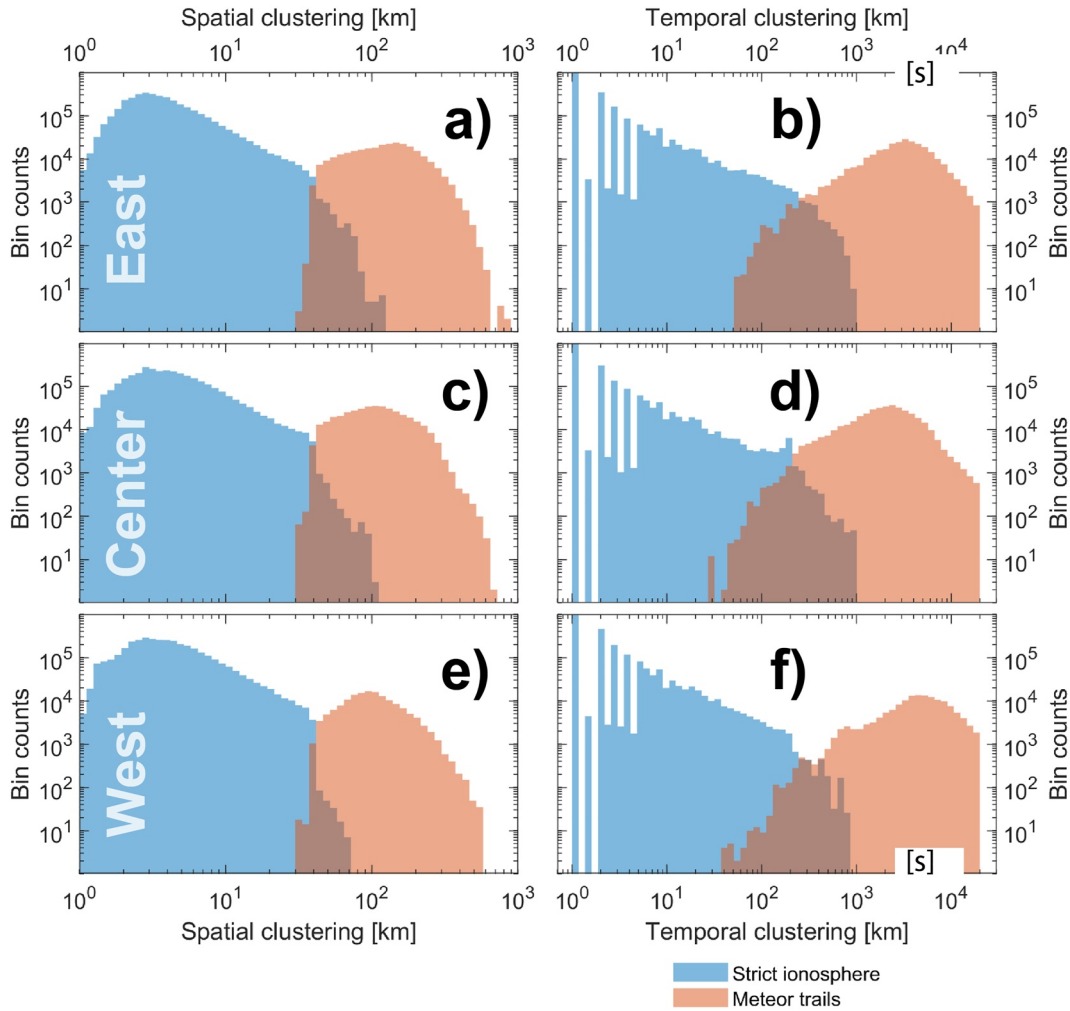

Figure 5. Spatial (panels a, c, e) and temporal (panels b, d, f) clustering for 13 million of the 160 million echoes recorded by ICEBEAR 3D in the period 2020, 2021. Strict ionospheric echoes are shown in blue while meteor trail echoes are shown in orange.

into the bottom-left and top-right corners of Figure 3b only, not considering the unclassified echoes for now, as their physical origin is not clearly identifiable.

Figure 4 sheds some additional light on the temporal evolution of the two types of echoes captured by ICEBEAR on 19 February 2021. It can be used to establish that the two classes of echoes do indeed originate from completely different mechanisms. In that figure the *y*-axis of panel (b) provides the number of echoes recorded per 3 min of operation, and the two *x*-axes give the time in UT and magnetic local time (MLT) at the radar bisector, again using the altitude-adjusted corrected geomagnetic coordinates system (Baker & Wing, 1989). Panel (a) shows the upper (SMU) and lower (SML) envelope of the SuperMAG index, quantifying disturbances in the auroral electrojet and overall auroral activity (Newell & Gjerloev, 2011). It can be seen that at earlier than local geomagnetic dusk (until just before 18hr MLT), no meteor trail echoes are recorded. The rate at which meteor trails are detected then rises steadily as ICEBEAR approaches geomagnetic dawn, with a peak occurrence at around 6hr MLT shortly before the radar operation ceased that day. "Strict ionosphere" echoes, on the other hand, are recorded in abundance only during a large burst of 90 min duration around geomagnetic midnight. During that time interval, the rate of incoming ionospheric echoes is more than 3 or 4 orders of magnitude higher than that of the meteor trail echoes. A short burst of ionospheric echoes is also recorded around 4hr MLT. Though appropriate local E-region ionization rates and electric field strength are needed, the SM-index in Panel (a) shows that the two periods of ionospheric echo detection coincide with enhancements in SMU and SML respectively.

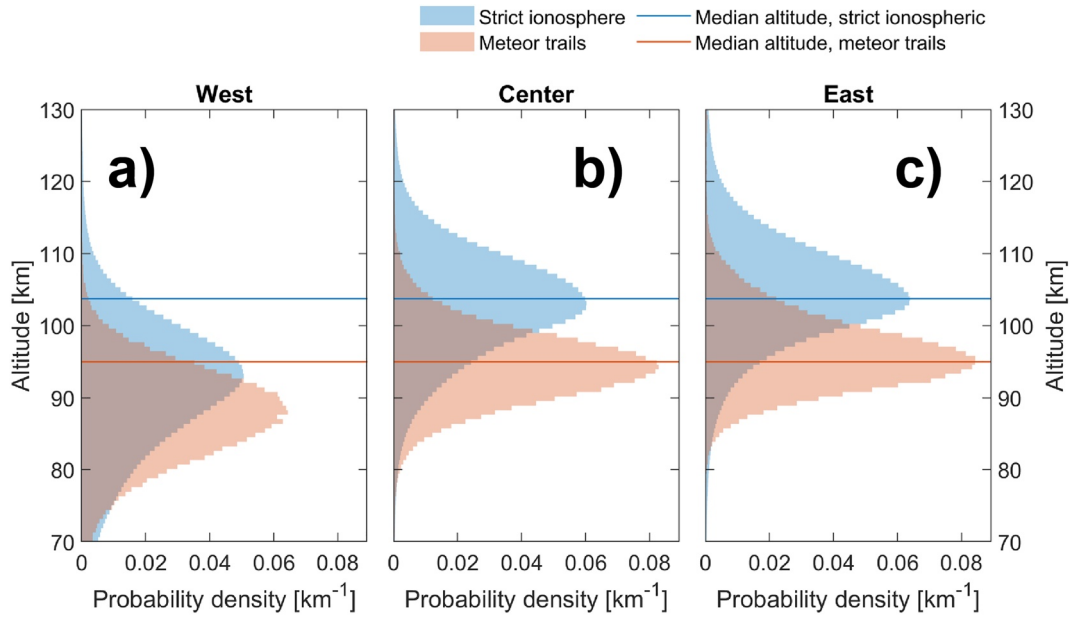

Figure 6. Altitude statistics for all echoes recorded by ICEBEAR 3D in the period 2020, 2021. Strict ionospheric echoes are shown in blue while meteor trail echoes are shown in orange. Panels (a), (b), and (c) correspond to the west, center, and east beams respectively.

3. Results

Using the algorithm described in the previous section, including discarding unclassified echoes, we gathered statistical information on a 13 million echoes subset. More specifically, in Figure 5 we show the total spatial (panels a, c, and e) and temporal (panels b, d, and f) cluster distributions for 11.8 million strict ionosphere echoes and 1 million meteor trail echoes (close to 11% of the total ICEBEAR 3D database from 2020, 2021). Clearly, the two populations of echoes are well separated, with strict ionospheric echoes exhibiting a median distance between 512 nearest neighbors of around 3 km in space and 1 s in time (recall that 1 s is the lowest temporal separation assigned in the algorithm, and that, for this resolution, most ionospheric echoes are in fact occurring simultaneously in time with their 512 nearest neighbors). By contrast, a typical meteor trail echo is on average separated by around 100 km spatially, and 50 min temporally, from its 512 nearest neighbors. This natural tendency for hugely different cluster scales in the echoes of ionospheric vs. meteoric origin allows for a robust method to automatically classify large high density radar data sets of the kind obtained by ICEBEAR 3D.

Figure 6 shows the altitude probability distributions, where the probability density for each bin is calculated as PDF $= c/(Nw)$, where c is the number of elements in each bin, N is the total number of elements, and w is the width of the bin. With this definition, the integral over PDF yields the dimensionless number 1. The distributions are shown for the strict ionosphere (blue) and meteor trail (orange) classes, for all 131 million data points in the 2020, 2021 ICEBEAR 3D database. Comparing Figures 1 and 6 demonstrate that the expectations of a central overlap region proved correct. In all three panels of Figure 6, blue and orange horizontal lines indicate the median altitude for strict ionosphere and meteor trail echoes respectively, calculated from the east and center beams only. Those altitudes are 104.1 km for the strict ionsphere echoes and 95.2 km for the meteor trail echoes. For the west beam, on the other hand, the median altitude for "strict ionosphere" echoes is around 93 km, with the meteor trail echoes peaking at around 89 km altitude. This difference—plus the fact that the center and east beams agree well with many observations from the past- shows that the west beam produces echoes that are significantly lower in altitude than those of the two other beams. The origin of the discrepancy has to be related to distortions in the antenna beam pattern owing to environmental circumstances such as topography and vegetation. Suitable corrections/modifications are in progress.

In Figure 7 we show a statistical aggregate of *rates* at which ionospheric and meteor trail echoes are detected by ICEBEAR, after binning the entire data set in 3-min segments. In panel (a) we show the total number of 3-min bins sorted by MLT at the radar bisector, where we see that ICEBEAR operation is more or less continuous between

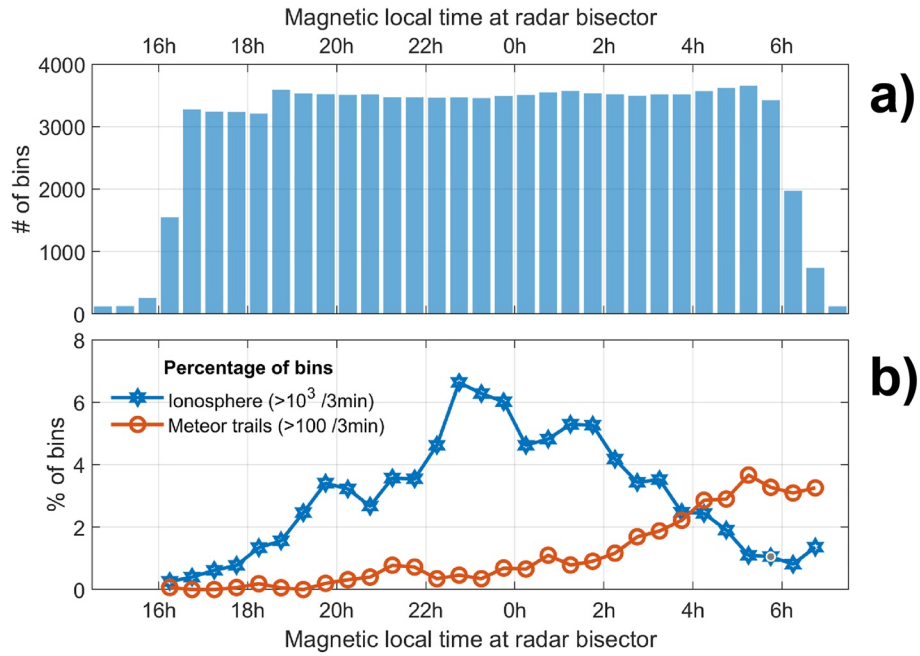

Figure 7. Statistical rates of echo detection, after binning the entire data set in 100,000 unique 3-min time segments. Panel (a) total number of 3-min bins sorted by magnetic local time at the radar bisector. Panel (b) proportion of bins exhibiting a rate of echo arrival greater than the indicated thresholds. See text for details.

16 and 6hr MLT every night. In panel (b), we show the proportion of bins exhibiting a rate of echo arrival greater than a threshold, for each MLT. Here, we show the proportion of ionospheric bins with greater than 1,000 echoes/3 min and the proportion of meteor trail bins with greater than 100 echoes/3 min, where the thresholds are implemented to filter our bins with an insignificantly small number of relevant echoes. We see that the rate of meteor trail echoes follows the pattern observed in Figure 4 with meteor trail echoes becoming gradually more and more common from dusk to dawn, a consequence of Earth's rotation with respect to its orbit around Sun. The ionospheric echoes, on the other hand, show a clear peak occurrence around magnetic midnight. This is due to the auroral oval being elongated toward lower MLATs toward magnetic midnight. At dusk and dawn, ICEBEAR's magnetic latitude (the radar bisector is located at 61° MLAT) is simply too low to frequently observe ionospheric echoes. When the oval expands during strong geomagnetic events ICEBEAR is then in a good position to detect ionospheric echoes at dusk and dawn.

4. Discussion

Figure 5 shows that the two classes of echoes are clearly separated in their degree of clustering by several orders of magnitude. While the figure reveals a portion with overlap between the two classes, the peaks of each distribution are several orders of magnitude higher than the overlapping portions. In other words, seeing clearly separated ionospheric and meteoric echoes in the ICEBEAR 3D data set is a thousand times more probable than seeing overlapping echoes.

The clear separation in Figure 5 agrees with earlier studies that have found coherent scatter echoes from meteor trails to appear grainy when observed on time-range-intensity plots of high enough resolution (Hall et al., 1997; Ponomarenko & Waters, 2006). By contrast, ionospheric instabilities vary smoothly over an extended region of space, meaning no sharp cutoff in the source of turbulence inside a region of auroral scattering at least in the case of non-ambivalent data subsets (i.e., ambient electric fields that are sufficiently uniform and above threshold for the trigger of Hall-current induced instabilities).

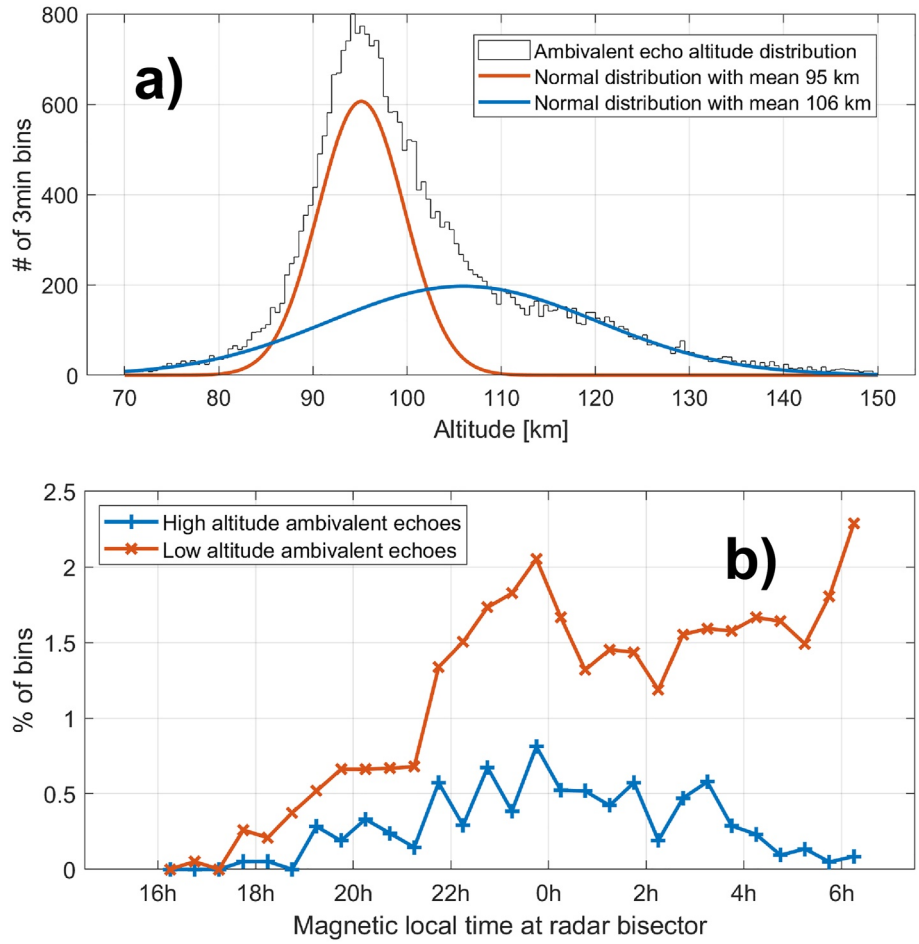

Figure 8. Panel (a) altitude distributions of all binned unclassified echo altitudes, using median altitude in each bin. Overall altitude distribution shown with a black line. Normal distributions with means of 95 and 106 km shown through orange and blue traces respectively. Panel (b) magnetic local time arrangement of unclassified echoes for high-altitude unclassified echoes (blue) and low-altitude unclassified echoes (orange), using 102 km altitude to separate the populations (the altitude intersection between the orange and blue curves in panel a). The *y*-axis represents the proportion of unclassified bins with a rate exceeding 100 echoes/3 min.

4.1. Limitations on the Meteor Subpoplation

We recall that our proposed meteor trail class of echoes is restricted to echoes with Doppler shift magnitudes <90 m/s. This requirement characterizes echoes from *specular* meteor trail echoes, which is the most conventional source of radar observations of meteors and justifies the use of meteor echoes to probe neutral winds (Zeng et al., 2022). However, when meteors explode or fragment while entering Earth's atmosphere, they can produce non-specular echoes (Oppenheim, Dyrud, & Ray, 2003; Zhu et al., 2016). Non-specular meteor trail echoes constitute what can be considered a dominant phenomenon in the meteor-atmosphere interaction (Mathews et al., 2010), but the topic is subject to an ongoing debate (Zhu et al., 2016). All such faster echoes are however 'unclassified' echoes in our classification algorithm, illustrated by the echoes occurring in the top left and bottom right quadrants of Figure 3b. Note that particularly strong neutral wind events with speeds in excess of 90 m/s will also lead to specular meteor trail echoes to be unclassified.

To shed some light on the origin of unclassified echoes, and to discuss the limitations of our classification algorithm's ability to detect meteor trail echoes, we present Figure 8. Here, we show statistics pertaining to unclassified echoes, where we again use 100,000 3-min long time segments collected during 2020, 2021. Panel (a) shows the altitude distributions of all binned unclassified echo altitudes, using median altitude in each bin. We see clearly that the overall altitude distribution (black line) can be accurately described by a very wide high-altitude normal distribution with 106 km mean (blue line) and a narrow low-altitude normal distribution with 95 km mean

(orange line). In panel (b), we show the occurrence of unclassified echoes as a function of MLT, and show the distinction between the high-altitude unclassified echo population (blue) and the low-altitude unclassified echo population (orange), on each side of 102 km altitude (the intersection between the blue and orange lines in panel (a)). Only the proportion of bins with a rate exceeding 100 echoes/3 min is shown. It can be seen that high-altitude unclassified echoes peak near geomagnetic midnight while low altitude unclassified echoes have a dual peak near geomagnetic midnight and at dawn. From this, we can conclude that the high-altitude unclassified echoes are of ionospheric origin, but that their occurrence is much lower than that of conventional ionospheric echoes (being no more abundant that 0.5% of the total). Likewise, we can conclude that the low-altitude unclassified echoes are largely meteoric in origin except around midnight, when a significant proportion of unclassified echoes below 102 km matches the maximum occurrence of auroral echoes, implying a contribution from ionospheric turbulence as well. Since we cannot accurately separate the ionospheric and meteoric unclassified echoes based on either clustering or altitude, a detailed study of unclassified echoes is left for future work.

A limitation of the algorithm's ability to accurately detect ionospheric echoes is the "drowning out" of meteor trail echoes during particularly strong events: when ionospheric echoes are coming in at a very high rate, all meteor trail echoes coming in at the *same patch of the sky* will be falsely classified as ionospheric in origin since their spatial and temporal separation will not be high enough to allow for proper classification. An example of this is shown in Figure 4, where we see that the rate of meteor trail echoes momentarily goes to zero at around 07:30 UT, when the rate of strict ionospheric echoes is sustained at rates exceeding 10^4/5 min, and is seen coming from all directions. However, at such times, correctly classified ionospheric echoes will vastly outnumber the concurrent meteor trail echoes (the blue bars in Figure 4 are more than three orders of magnitude higher than the orange bars). This limitation then leads to no real disadvantage to the analysis of ionospheric echoes. Correspondingly, echoes from meteor trails cannot be identified or handled when this happens, meaning that the study of meteor trail echoes should best be carried out at first during quiet geomagnetic times, as would be expected.

4.2. An Explanation for the Altitude Distribution of Echoes From Ionospheric Turbulence at 50 MHz

It is expected that plasma irregularity echoes from the E-region should, for the most part, be associated with the Farley-Buneman waves at 50 MHz, that is, at meter-size wavelengths (e.g., Hysell, 2015 and references therein). Phenomenologically, the likelihood of strong electric fields is increasingly smaller as the strength increases above 10 mV/m in auroral regions (St.-Maurice et al., 1976). In the absence of substantial heating of ions or electrons for electric fields weaker than 40 mV/m, the ion-acoustic speed is of the order of 350–400 m/s at altitudes ranging between 100 and 110 km. This means that at the very minimum an electric field of 18 mV/m must be present to excite Farley-Buneman waves through Hall currents, that is, for the magnitude of the ExB drift to exceed the ion-acoustic speed. For instabilities to be sufficiently developed in order to be seen over a wide enough region of space would therefore require roughly an electric field of 20 mV/m or more. This stated, with 20 mV/m fields being far more frequent than stronger electric fields, one should expect the upper altitude to normally be less than 110 km, with stronger amplitude waves in the region where the ion-acoustic speed is closer to 350 m/s, namely near 105 km. We have to emphasize the word "normally", since much interest lies into strong to very strong electric fields in spite of the fact that such fields are much rarer. The point here is not about predicting the altitude but to establish that when they are excited, unstable plasma waves should appear most frequently near 105 km altitude. We also have to keep in mind that stronger electric fields are required to excite plasma waves below 100 km altitude, because the electron Pedersen currents become important enough to limit the growth (e.g., Dimant & Sudan, 1995; Fejer & Kelley, 1980; Kissack et al., 1995; St.-Maurice & Chau, 2016). This all means that the *preferred* altitude for the observation of unstable waves produced by Hall currents is between 100 and 110 km, which agrees extremely well with the ICEBEAR 3D observations from the center and east beams.

4.3. Meteor Trail Altitude Distributions

Figure 6 shows that the meteor and ionospheric turbulence classes of echoes are well separated in altitude, with, as expected, a large enough spread in each category to introduce a population overlap between 90 and 105 km altitudes. The meteor population peak, near 95 km, turns out to be 9 km lower than the ionospheric instability population peak. A comparison with other radars of similar frequency dealing with specular meteor echoes indicates that our meteor peak altitude appears to be a few km higher than could have been expected. However, if we were to decrease our retrieved altitudes by this many km, the ionospheric altitude determination would not make sense, based on the expectations discussed in the previous subsection.

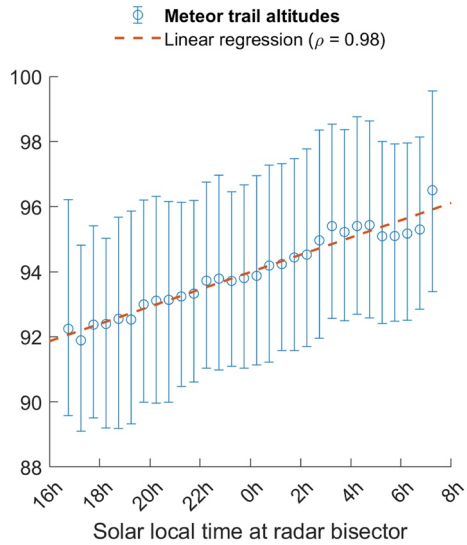

Figure 9. Median altitudes of meteor trails in 97,000 3-min segments, binned by solar local time at the radar bisector. Blue errorbars denote upper and lower quartile distributions, and a dashed orange line shows the result of a linear regression.

Going back to standard meteor radars: a basic expectation from those that study ordinary specular echoes from long ionization trails is that the lower the operating frequency of a radar is, the higher the detected altitude will be. This is based on diffusion arguments (Equation 1): the lower the frequency, the larger the wavelength and the longer it takes for a trail to decay so that trails become more visible higher up at lower frequencies. This is confirmed by observations, with 50 MHz radars producing echoes below 95 km while radars with few MHz frequencies can get echoes up to 105 km altitude and sometimes higher (Steel & Elford, 1991). More precise recent references that are consistent with this notion mention a peak occurrence at 92 km with a 31-MHz radar (Holdsworth et al., 2004), around 92 km with a 33-MHz radar (Lee et al., 2016), and around 90 km for a 52-MHz radar (Su et al., 2014), to take a few examples. However, keep in mind that meteor trail altitudes as measured by radar can exhibit considerable variation according to geographic location and local season (Liu et al., 2017).

The bistatic set up of ICEBEAR cannot account for a 5 km altitude difference with other 50 MHz systems. The wavelengths differences with these other radars are simply too small. This leaves the "look direction" of ICEBEAR 3D as the main likely culprit. ICEBEAR 3D looks in the northward direction at very low elevation angles. This contrasts with normal meteor radars that obtain data nearer the zenith and from all azimuths, which means that the bulk of the specular echoes observed by standard meteor radars is from trails that are relatively horizontal, albeit crossing the sky in any direction. By contrast, the field of view of ICEBEAR is such that it preferentially observes specular meteor echoes either from nearly vertical directions or from east-west trails that may be nearly horizontal or have a strong vertical tilt.

Due to the motion of the earth in the ecliptic plane the radar beams sweep through different sporadic meteor sources. The result is that on the morning side the relative energy of the meteoroids is much greater than for the evening side. In fact, at dusk there is less relative energy coming from impacts aligned with the earth motion than from the other directions, owing to the sweeping action of the planet. This means that on the morning side the fastest meteoroids come from directions that are closely aligned to the vertical, whereas the opposite is true for the evening sector. For ICEBEAR this will mean that the fastest meteoroids will be from nearly vertical trails in the morning sector and more (though not completely) horizontal east-west trails in the evening sector. Moreover, the energy of the meteoroids will be less in the evening sector. By contrast, standard meteor radars will tend to see relatively more horizontal trails at all times, with somewhat less energy and vertical tilt in the evening as opposed to the morning sector.

The above discussion has a strong impact on the statistical properties of the meteor counts and altitude. It is now recognized as a fact that the larger the energy, the higher the altitude of the meteor trails will be (Campbell-Brown, 2015). Therefore, ICEBEAR will see higher altitudes in the morning, owing to its capability to see near vertical trails. Said altitudes at that time of day will also be higher than observed by standard meteor radars, since the latter do not observe trails with large altitude tilts. However, for the evening side, ICEBEAR will collect mostly east-west trails that are more horizontal. These trails will also be produced by less energetic meteoroids and therefore will be seen at a lower altitude which should be comparable to the altitudes observed with standard meteor radars. The count contrast between morning and evening will, however, be rather large for ICEBEAR since it will only detect a fraction of the trails in the evening sector, owing to the viewing conditions.

In summary to the above discussion, we surmise that ICEBEAR should observe higher altitudes than standard radars in the morning sector and should see a much smaller meteor trail count in the evening as opposed to the morning. An important consequence is that on average, the bulk of the meteor echoes will be seen in the morning with ICEBEAR, in agreement with Figure 9. Given that state of affair, the other consequence will be that ICEBEAR will observe higher meteor altitude echoes on average than standard radars operating at a similar frequency.

It is indeed the case that ICEBEAR not only sees far more echoes in the morning sector but that it also detects a substantial variation in altitude with local time. Figure 9 shows the median altitudes of 97,000 3-min segments (selected based on having a ionospheric echo occurrence rate lower than 1,000 echoes/3 min), binned by solar

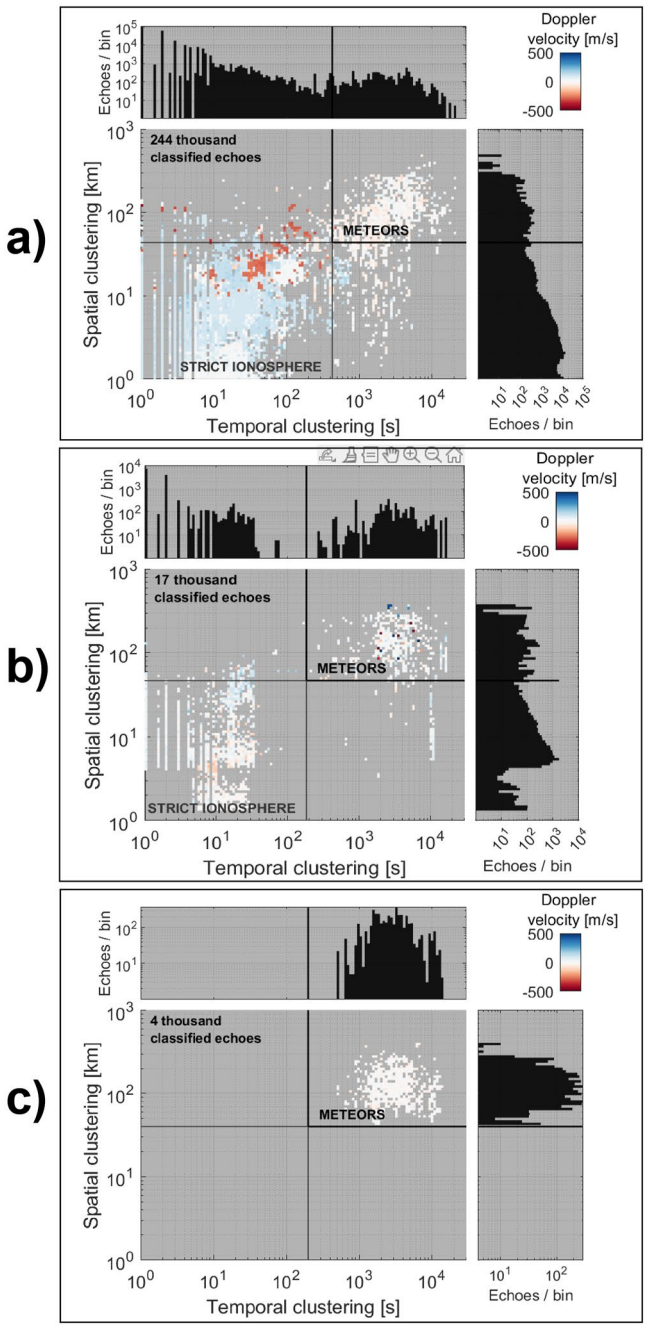

Figure 10. Three additional examples of echo classification analysis, from 15 January 2020 (panel a), 21 December 2021 (panel b), and 10 November 2020 (panel c). See Figure 3 for detailed key.

local time. Blue error bars denote upper and lower quartile distributions, and a dashed orange line shows the result of a linear regression, which yields a correlation coefficient of 0.98. This strongly supports the notion that the bulk of the meteor trails recorded by ICEBEAR comes from near vertical trails in the morning. It also explains why the median altitude is closer to 95 km than 90 km, given that the bulk of the echoes come from the morning sector (Figure 7b).

The above discussion notwithstanding, it is challenging to make accurate statements about the entry angle of meteors observed by ground-based radars. To validate the above chain of argument, we suggest future work should include the calculation of great circle radiant maps (Jones & Jones, 2006). As the contents of Figure 9 are completely new—we have not seen similarly clear and unequivocal local time variations in radar-based meteor trail altitude observations—such future work might prove useful for the community.

4.4. What Is Happening With the West Beam?

Figure 6 clearly shows that the west beam determination is producing altitudes that are systematically lower than that of the other two beams. By inspecting the overlapping transmitter array and receiver antenna gain patterns, it becomes apparent that the west beam defined in Figure 2 is being split by a region where a directivity null in the transmitter aray is aligned with another null in the receiver antenna. This creates an angle of arrival direction with lower power, similar to the areas between each beam in Figure 2. The problem of correcting the west beam anomaly is being dealt with in a separate paper, where topography and vegetation issues are considered along with antenna null patterns and antenna spacing.

4.5. Example to Show That Ionospheric Turbulence With Small Doppler Shifts Can Be Identified

Echoes from ionospheric turbulence typically have the ion-acoustic speed, C_s for their maximum phase velocity. Such waves have traditionally been labeled as "Type I." However, the turbulence also introduces modes that can have down to zero Doppler shifts. These wave were recognized from the earliest days of radar detection of Farley-Buneman waves and have been labeled as "Type II" waves (e.g., Fejer & Kelley, 1980). This means that there is a strong overlap between meteor echoes not just in altitude but also in Doppler shift. We now show that the two populations can nevertheless be well separated with our classification algorithm.

In Figure 10 we present three additional analyzed days of ICEBEAR 3D data. In panel (a), we see 244,000 analyzed echoes from 15 January 2020, of which the vast majority are slow (<200 m/s) strict ionosphere echoes, with a contingency of faster (<−200 m/s) redshifted echoes. Panel (b) shows 17,000 analyzed echoes from 21 December 2021, with an equal mix of slow (<150 m/s) strict ionosphere echoes and meteor trail echoes, while, by contrast, panel (c) shows 4,000 meteor trail echoes recorded on 10 November 2020.

Panels (a) and (b) clearly show that echo Doppler shift alone is not sufficient to distinguish between echoes of ionospheric and meteoric origin, whereas the clustering algorithm successfully distinguishes between the two phenomena. In both panels, the majority of the echoes are found in either the bottom left or top right quadrants, though a smaller number of echoes still have to be "unclassified."

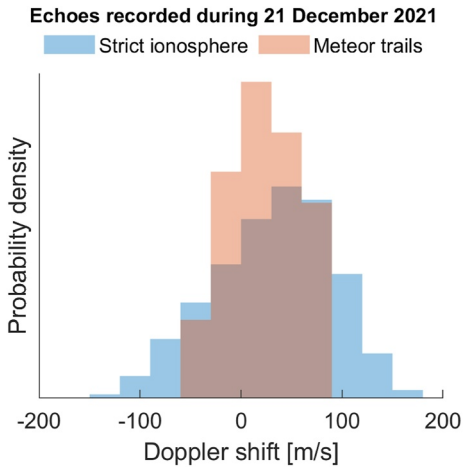

Figure 11. The distribution in Doppler shift for the two populations of echoes shown in Panel (b) of Figure 10.

To further illustrate the Doppler spectra associated with the two populations of echoes shown in Panel (b), we show in Figure 11 the distribution in Doppler velocities for the two populations. We see that whereas the first moments (means) of the two distributions are similar, the second moment (the variance) is not: the strict ionosphere echoes exhibit a standard deviation of 60 versus 35 m/s for the meteor trail echoes.

In panel (c) of Figure 10, we see a typical day in which ICEBEAR recorded only meteor trail echoes, which is to be expected under weak electric field conditions when Farley-Bunenan waves cannot be excited. In such situations, our proposed algorithm successfully classifies all echoes as meteor trail echoes by application of the threshold clustering values.

4.6. How to Choose the Right Window Sizes

Finally, to illustrate the effect of varying the temporal window size during which spatial clustering is calculated, we present in Figure 12 two illustrative cases based on Panel (c) of Figure 10. We see that the effect of reducing the spatial clustering-window size from 4 hr to 30 min is to drastically reduce the median distance between meteor trail echoes (Note that only the spatial clustering is affected by the window size, and that temporal clustering is calculated without any moving window in time). The reason for this is the relative temporal sparseness with which meteor trail echoes appear. If the window size is not long enough, there will simply not be 512 neighbors with which to compare, and the median spatial separation can be arbitrarily small. Increasing the window size ensures that enough neighbors are taken into account to produce an accurate estimate of the spatial clustering of meteor trail echoes. All parameters in the proposed algorithm have been subject to extensive testing.

5. Conclusion

We have developed a new algorithm to automatically separate meteor echoes from ionospheric turbulence echoes in regions where the two types overlap. This proves useful when the two types co-exist or when the dominant type changes during longer periods of observations. The new scheme is based on the natural tendency for each type to cluster very differently in space and time. The algorithm was developed and tested through an extensive database from ICEBEAR 3D containing 131 million echoes at 1 s resolution. While the idea behind the classification scheme is not new (it has been successfully performed in the past), the chief advantage of the modification introduced by our method is that it allows for an easy and automatic classification of millions of individual backscatter echoes, thereby making it particularly suitable for coherent radar systems that produce high data rates with a high density of radar echoes.

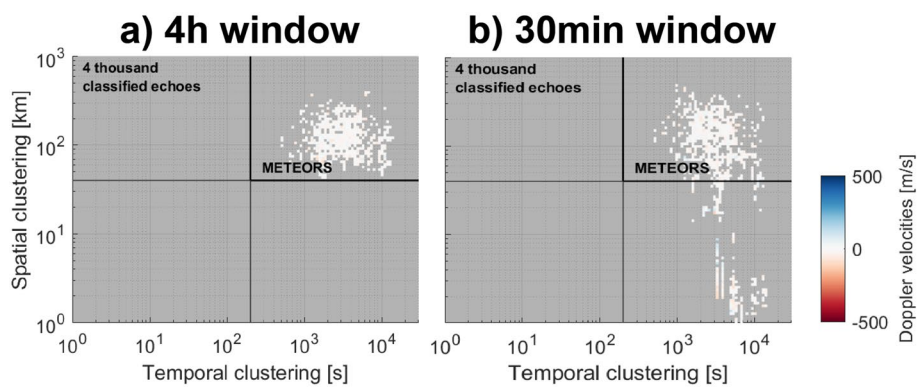

Figure 12. Echo classification for all echoes recorded during 10 November 2020 (panel c of Figure 10), with a varying window size during which spatial clustering is calculated. Panel (a) uses a window size of 4 hr, while Panel (b) uses a window size of 30 min. Note that only the spatial clustering is affected by the window size, and that temporal clustering is calculated without any moving window in time.

The database included echoes positions in space, in addition to other characteristics such as SNR and Doppler shift. We successfully tested the classification algorithm for a variety of circumstances. We obtained statistical results of the clustering algorithm for the entire database of ICEBEAR 3D echoes from 2020, 2021, from which we could infer basic clustering scales in time and space, after which we could infer the altitude properties for each echo population. We found 105 km to be the preferred altitude for ionospheric turbulence, in agreement with theoretical expectations based on instabilities triggered by high latitude Hall currents (accurate observations of the preferred altitudes for these instabilities are lacking in the literature). The preferred altitude for meteor echoes was 9 km lower. Also as expected, the echoes from ionospheric turbulence were the only ones to have Doppler shifts in excess of 100 m/s. While the meteor trail echo class only contain echoes slower than 90 m/s, a large sub-population from ionospheric turbulence also had small Doppler shifts, again as expected from numerous previous studies.

During meteor showers, meteor trail echoes will stand to be much more crowded both in space and time, rendering the normal threshold values for clustering less effective. As the spatial and temporal clustering of echoes recorded during active meteor showers could approach that of ionospheric echoes, we made, for the time being, no attempt at classifying echoes during such events.

Another type of study left for future research is the "unclassified" class of echoes, where we have shown that both meteoric and ionospheric echoes co-exist, and thus were left to ambiguous interpretations. Although unclassified echoes can conceivably be associated with non-specular meteor trail echoes, these types of echoes might also be associated with fast ionospheric transients, as might be expected from Alfén wave reflection events.

Data Availability Statement

Daily ICEBEAR 3D data from 2020, 2021 is published with https://doi.org/10.5281/zenodo.7509022.

Acknowledgments
The authors are grateful to J Chau, M Campbell-Brown, G Stober, C Meek, J Vierinen, and D Huyghebaert for stimulating discussions. We acknowledge the support of the Canadian Space Agency (CSA) [20SUGOICEB; 21SUSTIERI CSA GO], the Canada Foundation for Innovation (CFI) John R. Evans Leaders Fund [32117] and the Province of Saskatchewan. We also acknowledge the support of the Natural Science and Engineering Research Council (NSERC) and the programs: the International Space Mission Training Program supported by the Collaborative Research and Training Experience (CREATE) [479771-2016] program and the Discovery Grants program [RGPIN-2019-19135]; and the Digital Research Alliance of Canada [RRG-FT2109].

References

Abel, W. G., & Newell, R. E. (1969). Measurements of the afternoon radio aurora at 1295 MHz. *Journal of Geophysical Research (1896-1977)*, *74*(1), 231–245. https://doi.org/10.1029/JA074i001p00231

Baker, K. B., & Wing, S. (1989). A new magnetic coordinate system for conjugate studies at high latitudes. *Journal of Geophysical Research*, *94*(A7), 9139–9143. https://doi.org/10.1029/JA094iA07p09139

Barnes, A. A. (1973). Status report on radar meteor wind and density measurements. *Bulletin of the American Meteorological Society*, *54*(9), 900–911. https://doi.org/10.1175/1520-0477(1973)054⟨0900:SRORMW⟩2.0.CO;2

Bourdillon, A., Haldoupis, C., Hanuise, C., Le Roux, Y., & Menard, J. (2005). Long duration meteor echoes characterized by Doppler spectrum bifurcation. *Geophysical Research Letters*, *32*(5), L05805. https://doi.org/10.1029/2004GL021685

Buneman, O. (1963). Excitation of field aligned sound waves by electron streams. *Physical Review Letters*, *10*(7), 285–287. https://doi.org/10.1103/PhysRevLett.10.285

Campbell-Brown, M. (2015). A population of small refractory meteoroids in asteroidal orbits. *Planetary and Space Science*, *118*, 8–13. https://doi.org/10.1016/j.pss.2015.03.022

Chau, J. L., & St.-Maurice, J.-P. (2016). Unusual 5 m E region field-aligned irregularities observed from Northern Germany during the magnetic storm of 17 March 2015. *Journal of Geophysical Research: Space Physics*, *121*(10), 10316–10340. https://doi.org/10.1002/2016JA023104

Dimant, Y. S., & Sudan, R. N. (1995). Kinetic theory of low-frequency cross-field instability in a weakly ionized plasma. I. *Physics of Plasmas*, *2*(4), 1157–1168. https://doi.org/10.1063/1.871394

Farley, D. T. (1963). A plasma instability resulting in field-aligned irregularities in the ionosphere. *Journal of Geophysical Research (1896-1977)*, *68*(22), 6083–6097. https://doi.org/10.1029/JZ068i022p06083

Fejer, B. G., & Kelley, M. C. (1980). Ionospheric irregularities. *Reviews of Geophysics*, *18*(2), 401–454. https://doi.org/10.1029/RG018i002p00401

Galeschuk, D. T. K. (2021). Verification and calibration of the ICEBEAR radar through GPU acceleration, noise characterization and calculation, and radio galaxy phase calibration (Thesis, University of Saskatchewan). Retrieved from https://harvest.usask.ca/handle/10388/13427

Haldoupis, C. (1989). A review on radio studies of auroral E-region ionospheric irregularities. *Annales Geophysicae*, *7*, 239–258.

Hall, G. E., MacDougall, J. W., Moorcroft, D. R., St.-Maurice, J.-P., Manson, A. H., & Meek, C. E. (1997). Super dual auroral radar network observations of meteor echoes. *Journal of Geophysical Research*, *102*(A7), 14603–14614. https://doi.org/10.1029/97JA00517

Hargreaves, J. K., & Hunsucker, R. D. (2002). Radio techniques for probing the ionosphere. In *The high-latitude ionosphere and its effects on radio propagation* (pp. 181–226). Cambridge University Press. https://doi.org/10.1017/CBO9780511535758.006

Holdsworth, D. A., Reid, I. M., & Cervera, M. A. (2004). Buckland park all-sky interferometric meteor radar. *Radio Science*, *39*(5). https://doi.org/10.1029/2003RS003014

Hussey, G. C., Meek, C. E., André, D., Manson, A. H., Sofko, G. J., & Hall, C. M. (2000). A comparison of northern hemisphere winds using SuperDARN meteor trail and MF radar wind measurements. *Journal of Geophysical Research*, *105*(D14), 18053–18066. https://doi.org/10.1029/2000JD900272

Huyghebaert, D., Hussey, G., Vierinen, J., McWilliams, K., & St-Maurice, J.-P. (2019). ICEBEAR: An all-digital bistatic coded continuous-wave radar for studies of the E region of the ionosphere. *Radio Science*, *54*(4), 349–364. (Conference Name: Radio Science). https://doi.org/10.1029/2018RS006747

Hysell, D. (2015). The radar aurora. (pp. 191–209). https://doi.org/10.1002/9781118978719.ch14

Jenkins, B., Jarvis, M. J., & Forbes, D. M. (1998). Mesospheric wind observations derived from super dual auroral radar network (SuperDARN) HF radar meteor echoes at Halley, Antarctica: Preliminary results. *Radio Science*, *33*(4), 957–965. https://doi.org/10.1029/98RS01113

Jones, J., & Jones, W. (2006). Meteor radiant activity mapping using single-station radar observations. *Monthly Notices of the Royal Astronomical Society*, *367*(3), 1050–1056. https://doi.org/10.1111/j.1365-2966.2006.10025.x

Kero, J., Campbell-Brown, M. D., Stober, G., Chau, J. L., Mathews, J. D., & Pellinen-Wannberg, A. (2019). Radar observations of meteors. In G. O. Ryabova, D. J. Asher, & M. D. Campbell-Brown (Eds.), *Meteoroids: Sources of meteors on earth and beyond. Cambridge planetary science* (pp. 65–89). Cambridge University Press. https://doi.org/10.1017/9781108606462.008

Kissack, R. S., St-Maurice, J., & Moorcroft, D. R. (1995). Electron thermal effects on the Farley–Buneman fluid dispersion relation. *Physics of Plasmas*, *2*(4), 1032–1055. https://doi.org/10.1063/1.871383

Kumar, K. K. (2007). Temperature profiles in the MLT region using radar-meteor trail decay times: Comparison with TIMED/SABER observations. *Geophysical Research Letters*, *34*(16), L16811. https://doi.org/10.1029/2007GL030704

Larsen, M. F. (2002). Winds and shears in the mesosphere and lower thermosphere: Results from four decades of chemical release wind measurements. *Journal of Geophysical Research*, *107*(A8), SIA28–1–SIA28–14. https://doi.org/10.1029/2001JA000218

Larsen, M. F., Hysell, D. L., Zhou, Q. H., Smith, S. M., Friedman, J., & Bishop, R. L. (2007). Imaging coherent scatter radar, incoherent scatter radar, and optical observations of quasiperiodic structures associated with sporadic E layers. *Journal of Geophysical Research*, *112*(A6), A06321. https://doi.org/10.1029/2006JA012051

Lee, C., Kim, J.-H., Jee, G., Lee, W., Song, I.-S., & Kim, Y. H. (2016). New method of estimating temperatures near the mesopause region using meteor radar observations. *Geophysical Research Letters*, *43*(20), 10580–10585. https://doi.org/10.1002/2016GL071082

Li, G., Ning, B., Wan, W., Reid, I. M., Hu, L., Yue, X., et al. (2014). Observational evidence of high-altitude meteor trail from radar interferometer. *Geophysical Research Letters*, *41*(19), 6583–6589. https://doi.org/10.1002/2014GL061478

Li, G., Yan, J., & Lan, A. (2021). An improved meteor echo recognition algorithm for SuperDARN HF radar. *Electronics*, *10*(16), 1971. https://doi.org/10.3390/electronics10161971

Liu, L., Liu, H., Chen, Y., Le, H., Sun, Y.-Y., Ning, B., et al. (2017). Variations of the meteor echo heights at Beijing and Mohe, China. *Journal of Geophysical Research: Space Physics*, *122*(1), 1117–1127. https://doi.org/10.1002/2016JA023448

Lozinsky, A., Hussey, G., McWilliams, K., Huyghebaert, D., & Galeschuk, D. (2022). ICEBEAR-3D: A low elevation imaging radar using a non-uniform coplanar receiver array for E region observations. *Radio Science*, *57*(3), e2021RS007358. https://doi.org/10.1029/2021RS007358

Mathews, J. D., Briczinski, S. J., Malhotra, A., & Cross, J. (2010). Extensive meteoroid fragmentation in V/UHF radar meteor observations at Arecibo observatory. *Geophysical Research Letters*, *37*(4), L04103. https://doi.org/10.1029/2009GL041967

McKinley, D. W. R. (1961). *Meteor science and engineerin*g. McGraw-Hill. (Google-Books-ID: BSAIAQAAIAAJ).

Moisan, M., & Pelletier, J. (2012). Hydrodynamic description of a plasma. In M. Moisan & J. Pelletier (Eds.), *Physics of collisional plasmas: Introduction to high-frequency discharges* (pp. 203–335). Springer Netherlands. https://doi.org/10.1007/978-94-007-4558-2_3

Newell, P. T., & Gjerloev, J. W. (2011). Evaluation of SuperMAG auroral electrojet indices as indicators of substorms and auroral power. *Journal of Geophysical Research*, *116*(A12), A12211. https://doi.org/10.1029/2011JA016779

Oppenheim, M. M., Dyrud, L. P., & Ray, L. (2003). Plasma instabilities in meteor trails: Linear theory. *Journal of Geophysical Research*, *108*(A2), 1063. https://doi.org/10.1029/2002JA009548

Oppenheim, M. M., Dyrud, L. P., & vom Endt, A. F. (2003). Plasma instabilities in meteor trails: 2-D simulation studies. *Journal of Geophysical Research*, *108*(A2), 1064. https://doi.org/10.1029/2002JA009549

Ponomarenko, P. V., & Waters, C. L. (2006). Spectral width of SuperDARN echoes: Measurement, use and physical interpretation. *Annales Geophysicae*, *24*(1), 115–128. https://doi.org/10.5194/angeo-24-115-2006

Steel, D. I., & Elford, W. G. (1991). The height distribution of radio meteors: Comparison of observations at different frequencies on the basis of standard echo theory. *Journal of Atmospheric and Terrestrial Physics*, *53*(5), 409–417. https://doi.org/10.1016/0021-9169(91)90035-6

St.-Maurice, J.-P., & Chau, J. L. (2016). A theoretical framework for the changing spectral properties of meter-scale Farley-Buneman waves between 90 and 125 km altitudes. *Journal of Geophysical Research: Space Physics*, *121*(10), 10341–10366. https://doi.org/10.1002/2016JA023105

St. Maurice, J.-P., Foster, J. C., Holt, J. M., & Del Pozo, C. (1989). First results on the observation of 440-MHz high-latitude coherent echoes from the E region with the Millstone Hill radar. *Journal of Geophysical Research*, *94*(A6), 6771–6798. https://doi.org/10.1029/ja094ia06p06771

St-Maurice, J.-P., & Hamza, A. M. (2009). Small scale irregularities at high latitudes. In G. Wyman (Ed.), *Characterising the ionosphere*, *Technical report RTO-TR-IST-051. Neuilly-sur-Seine*. RTO.

St.-Maurice, J. P., Hanson, W. B., & Walker, J. C. G. (1976). Retarding potential analyzer measurement of the effect of ion-neutral collisions on the ion velocity distribution in the auroral ionosphere. *Journal of Geophysical Research (1896-1977)*, *81*(31), 5438–5446. https://doi.org/10.1029/JA081i031p05438

Stober, G., Jacobi, C., Matthias, V., Hoffmann, P., & Gerding, M. (2012). Neutral air density variations during strong planetary wave activity in the mesopause region derived from meteor radar observations. *Journal of Atmospheric and Solar-Terrestrial Physics*, *74*, 55–63. https://doi.org/10.1016/j.jastp.2011.10.007

Stober, G., Matthias, V., Brown, P., & Chau, J. L. (2014). Neutral density variation from specular meteor echo observations spanning one solar cycle. *Geophysical Research Letters*, *41*(19), 6919–6925. https://doi.org/10.1002/2014GL061273

Su, C. L., Chen, H. C., Chu, Y. H., Chung, M. Z., Kuong, R. M., Lin, T. H., et al. (2014). Meteor radar wind over Chung-Li (24.9°N, 121°E), Taiwan, for the period 10–25 November 2012 which includes Leonid meteor shower: Comparison with empirical model and satellite measurements. *Radio Science*, *49*(8), 597–615. https://doi.org/10.1002/2013RS005273

Sugar, G., Oppenheim, M. M., Bass, E., & Chau, J. L. (2010). Nonspecular meteor trail altitude distributions and durations observed by a 50 MHz high-power radar. *Journal of Geophysical Research*, *115*(A12), A12334. https://doi.org/10.1029/2010JA015705

Yukimatu, A. S., & Tsutsumi, M. (2002). A new SuperDARN meteor wind measurement: Raw time series analysis method and its application to mesopause region dynamics. *Geophysical Research Letters*, *29*(20), 42–1–42–4. https://doi.org/10.1029/2002GL015210

Zeng, L., Yue, X., Ke, C., Ding, F., Zhao, B., & Ning, B. (2022). Potential direct observation of meteoroid fragmentation by a high range resolution radar. *Icarus*, *372*, 114763. https://doi.org/10.1016/j.icarus.2021.114763

Zhu, Q., Dinsmore, R., Gao, B., & Mathews, J. D. (2016). High-resolution radar observations of meteoroid fragmentation and flaring at the Jicamarca radio observatory. *Monthly Notices of the Royal Astronomical Society*, *457*(2), 1759–1769. https://doi.org/10.1093/mnras/stw070